

A New Measurement of the 1S_0 Neutron-Neutron Scattering Length using the Neutron-Proton Scattering Length as a Standard

D.E. González Trotter¹, F. Salinas¹, Q. Chen¹, A.S. Crowell¹, W. Glöckle², C.R. Howell¹, C.D. Roper¹, D. Schmidt³, I. Šlaus⁴, H. Tang⁵, W. Tornow¹, R.L. Walter¹, H. Witała⁶ and Z. Zhou⁵

¹*Duke University and Triangle Universities Nuclear Laboratory, Durham, NC 27708, USA*

²*Institut für Theoretische Physik, Ruhr-Universität Bochum, D-44780 Bochum, Germany*

³*Physikalisch-Technische Bundesanstalt, D-38116 Braunschweig, Germany*

⁴*Rudjer Boskovic Institute, Zagreb, Croatia.*

⁵*Chinese Institute for Atomic Energy, Beijing, Peoples Republic of China*

⁶*Institute of Physics, Jagellonian University, PL-30059 Cracow, Poland*

(July 24, 2021)

The present paper reports high-accuracy cross-section data for the $^2\text{H}(n, nnp)$ reaction in the neutron-proton (np) and neutron-neutron (nn) final-state-interaction (FSI) regions at an incident mean neutron energy of 13.0 MeV. These data were analyzed with rigorous three-nucleon calculations to determine the 1S_0 np and nn scattering lengths, a_{np} and a_{nn} . Our results are $a_{nn} = -18.7 \pm 0.6$ fm and $a_{np} = -23.5 \pm 0.8$ fm. Since our value for a_{np} obtained from neutron-deuteron (nd) breakup agrees with that from free np scattering, we conclude that our investigation of the nn FSI done simultaneously and under identical conditions gives the correct value for a_{nn} . Our value for a_{nn} is in agreement with that obtained in π^-d measurements but disagrees with values obtained from earlier nd breakup studies.

25.10.+s,25.40.Fq

The difference in the 1S_0 neutron-neutron (nn) and proton-proton (pp) scattering lengths is an explicit measure of charge-symmetry breaking (CSB) of the nuclear force. The high sensitivity of these scattering lengths to the nuclear potential strength makes them a valuable probe for detecting small potential-energy contributions like the isospin-dependent forces [1–3] that cause CSB . For realistic potentials, a 1% change in the potential strength results in a 30% shift in the scattering length. Since it is not technically viable to measure a_{nn} directly by conducting free nn scattering experiments, one uses few-nucleon reactions that emit two neutrons with low relative momentum, i.e., a final-state interaction (FSI) configuration. The two reactions used to measure a_{nn} that have the smallest theoretical uncertainties are pion-deuteron capture ($\pi^- + d \rightarrow n + n + \gamma$) and neutron-deuteron breakup ($n + d \rightarrow n + n + p$). Curiously, measurements using these two reactions give significantly different values of a_{nn} : from π^-d capture measurements the average value for a_{nn} is -18.6 ± 0.4 fm [4–6] and from kinematically-complete nd breakup experiments the average value is -16.7 ± 0.5 fm [1]. It was suggested that the difference in these values has its origin in the three-nucleon force (3NF), which would act in the nd breakup reaction [1] but not in the other.

The goal of the present work was to measure a_{nn} with the nd breakup reaction to an accuracy better than ± 0.7 fm. To this aim a_{np} was measured simultaneously and used as a standard for evaluating our methods and for determining the influence of the 3NF in nd breakup. We obtained a_{np} and a_{nn} from absolute cross-section measurements in the np and nn FSI regions, respectively,

in nd breakup at an incident mean neutron energy of $E_n = 13.0$ MeV. Rigorous nd breakup calculations with the Tucson-Melbourne (TM) 3NF potential [7] show that the percentage change in np and nn FSI cross sections from the addition of a 3NF are equal. Based on this observation and the fact that a_{np} has been determined to high accuracy by np scattering [8], we used our extracted values of a_{np} to set an upper limit on the 3NF influence on the value of a_{nn} determined in the present experiment. Because 3NF effects might have a stronger energy and angle dependence than indicated by our calculations with the TM 3NF model, we designed the experiment to obtain nn FSI data at the same energy and angle configurations as that for the np FSI data. Furthermore, guided by our calculations of the angle dependence of 3NF effects on the NV FSI cross-section enhancement [9], measurements were made at several np and nn emission angles. The measured cross-section distribution at each np (nn) angle was used to determine a value of a_{np} (a_{nn}), and the predicted angle dependence of a_{np} (a_{nn}) due to 3NF effects was investigated.

All measurements were made using the shielded neutron source at the Triangle Universities Nuclear Laboratory (TUNL). The experimental setup is shown in Fig. 1. The momentum of the two emitted neutrons and the energy of the proton in each breakup event were measured, thereby overdetermining the kinematics. The neutrons were detected in liquid organic scintillators. The energy of the emitted proton was measured in the deuterated liquid scintillator C_6D_{12} (NE-232), which served as the deuteron scatterer and will be referred to as the central detector (CD). The energies of the outgoing neutrons

were determined by measuring their flight times from the CD to the neutron detectors. The neutron detectors on the right side of the incident beam axis were used for the nn FSI measurements. At each angle of the nn pair, one neutron was detected in the ring-shaped detector placed 1.5 m from the CD and the other in the coaxial cylindrical detector placed 2.5 m from the CD, which was positioned to fill the solid angle of the opening in the ring detector.

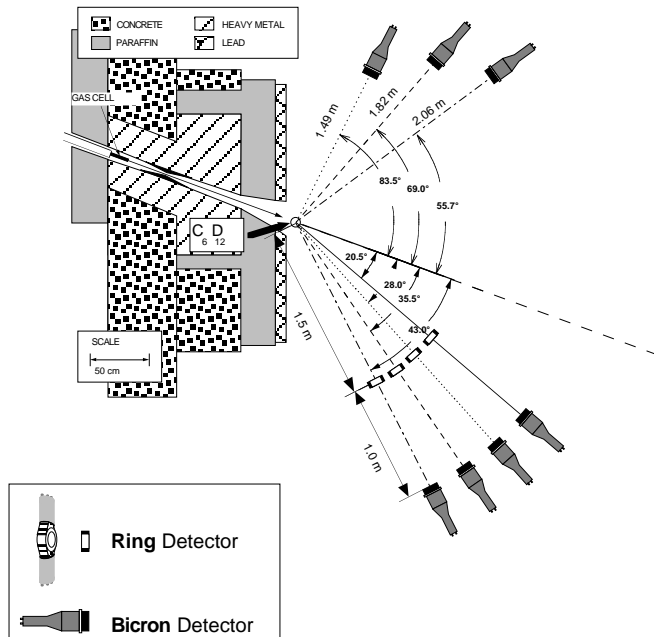


FIG. 1. The experimental setup for the NN FSI cross-section measurements in nd breakup. All detectors are in the horizontal plane. The two detectors used to measure the np FSI cross section at a specific np angle pair lie on lines of the same type. The nm FSI cross sections were measured at each angle with the pair of ring and cylindrical detectors positioned at that angle.

In the np FSI one neutron moves in the same direction as the proton, and the other one is emitted on the opposite side of the incident neutron-beam axis. The neutrons emitted on the right side were detected in either the ring-shaped detector or in the cylindrical detector. The associated neutrons were emitted to the left side and were detected in cylindrical scintillators located as shown in Fig. 1. All neutron detectors were filled with a liquid scintillator fluid with $n-\gamma$ pulse-shape sensitivity (either NE213 or BC501A). The active volume of each cylindrical detector was 12.6 cm dia. \times 5.5 cm thick, and that of each ring detector was 7.6 cm inner dia. \times 13.4 cm outer dia. \times 4.0 cm thick. The neutron detector efficiencies were determined in a dedicated series of measurements using neutrons from the ${}^2\text{H}(d, n){}^3\text{He}$ reaction and from a ${}^{252}\text{Cf}$ source. The energy dependence of the relative detection efficiency of each detector was determined to an accuracy of $\pm 1.0\%$, and the absolute efficiency to $\pm 2.5\%$. The neutron beam was produced using the ${}^2\text{H}(d, n){}^3\text{He}$

reaction. The production target was a 3-cm long cell pressurized with 7.8 atm of deuterium gas. The cell was bombarded with a 10.0-MeV d.c. deuteron beam, which entered the cell through a 6.35- μm thick Havar containment foil and was stopped in a gold end cap. The neutron energy spread was 400 keV. The detector area was shielded from the neutron production target by a 1.7-m thick multiple component wall. The neutron beam at the CD was defined by a rectangular double-truncated collimator, which was designed such that the CD was illuminated almost exclusively by unscattered neutrons produced in the deuterium gas cell. The deuteron beam current on target was about $2\ \mu\text{A}$, and the counting rate of the CD was about 400 kHz with a threshold setting of one-tenth of the Compton-scattering edge for γ rays from a ${}^{137}\text{Cs}$ source. The rate in the CD electronics set the limit on the maximum acceptable beam current. The pulse-height thresholds on the neutron detectors were set at one-third of the ${}^{137}\text{Cs}$ Compton-scattering edge. Data were collected for a total of 2000 hours.

The integrated beam-target luminosity was determined by measuring the yields for nd elastic scattering concurrently with the data from the breakup reaction. Since the differential cross section for nd elastic scattering can be calculated using realistic NN potentials in the Faddeev method with high numerical precision [10] and the calculations agree well with existing data, we elected to use calculated cross sections rather than experimental data in the luminosity determination. The simultaneous accumulation of the breakup and nd elastic-scattering data reduced the sensitivity of our measurements to system deadtimes and absolute detection efficiencies. Also this technique eliminated the need for absolute measurements of the neutron flux and the thickness of the CD.

The width of the coincidence window in the event-trigger circuit was 400 ns and allowed for the concurrent measurements of *true* breakup events and events due to the *accidental* coincidences between signals from the CD and the neutron detectors. All events that satisfied conservation of energy within ± 2 MeV were projected into 0.5-MeV wide bins along the point-geometry kinematic locus. The distance along the kinematic curve of E_{n1} versus E_{n2} , where E_{n1} and E_{n2} are the energies of the two emitted neutrons, will be referred to as S . The value of S is set to zero at the point where $E_{n2} = 0$ and increases as one moves counterclockwise around the locus. The *true+accidental* and *accidental* events were projected onto the ideal locus separately. The projection was done using the minimum-distance technique described by Finckh *et al.* [11]. The *true* events were obtained by subtracting *accidental* from *true+accidental* events.

The measured cross sections were compared to Monte-Carlo (MC) simulations that included the energy resolution and the finite geometry of the experimental setup. The basis of these simulations was theoretical point-geometry cross-section libraries generated for a range of

a_{np} (a_{nn}) values at incident neutron energies of 12.8, 13.0 and 13.2 MeV. The point-geometry cross sections were obtained from transition matrix elements of the breakup operator U_0

$$U_0 = (1 + P)\tilde{T}, \quad (1)$$

where the \tilde{T} operator sums up all multiple scattering contributions through the three-nucleon (3N) Faddeev integral equation

$$\begin{aligned} \tilde{T}|\phi\rangle &= tP|\phi\rangle + (1 + tG_0)V_4^{(1)}(1 + P)|\phi\rangle + tPG_0\tilde{T}|\phi\rangle \\ &+ (1 + tG_0)V_4^{(1)}(1 + P)G_0\tilde{T}|\phi\rangle. \end{aligned} \quad (2)$$

Here G_0 is the free 3N propagator, t is the NN t-matrix, and operator P is the sum of a cyclical and anticyclical permutation of three nucleons. In the generation of the libraries, the terms containing V_4 , the 3NF potential, were set to zero.

The cross-section libraries were obtained using the Bonn-B (OBEPQ) NN potential [12]. This potential is fitted in the 1S_0 state to the experimentally-determined value of a_{np} . The charge-independence breaking in the 1S_0 NN force is imposed by using for the 1S_0 nn force the version of the Bonn-B potential [12] that was fitted to pp data. To account for charge-symmetry breaking in the calculations, the total 3N isospin $T=3/2$ admixture has been included [13]. For the purpose of this analysis, modifications of the 1S_0 NN interaction were accomplished by adjusting the σ -meson coupling constant $g_\sigma^2/4\pi$ [12]. In this way 1S_0 np (nn) interactions with different np (nn) scattering lengths were generated.

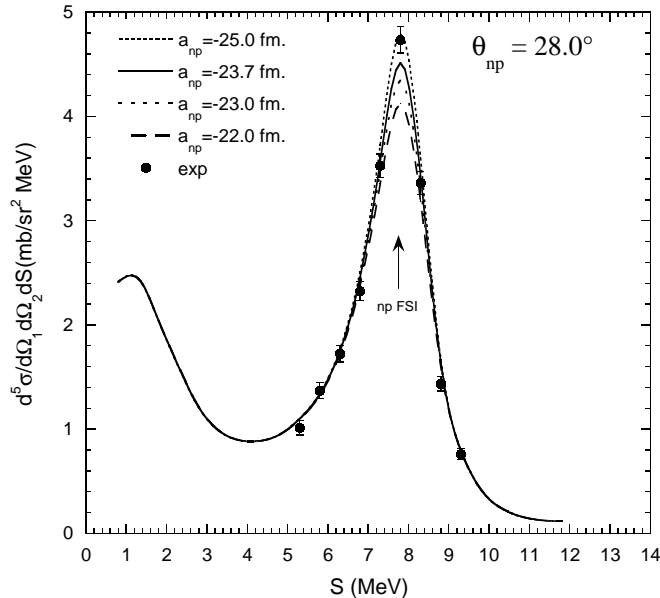


FIG. 2. Cross sections for $\theta_{np} = 28.0^\circ$ ($\theta_{n1} = 28.0^\circ$, $\theta_{n2} = 83.5^\circ$, $\phi_{12} = 180^\circ$). The points are the data from the present work. The curves are MC simulations based on nd calculations made with four values of a_{np} : -22.0, -23.0, -23.75 and -25.0 fm.

Simulated cross sections in comparison to our data for 28.0° are shown in Figs. 2 and 3 for several values of a_{np} and a_{nn} , respectively. A value of a_{NN} and its statistical uncertainty were determined for each detector-pair configuration using a single-parameter (either a_{np} or a_{nn}) minimum- χ^2 fit to the absolute cross-section data. The results are given in Table I. The uncertainties listed in Table I are statistical only. The systematic uncertainties in our determinations are ± 0.8 fm for a_{np} and ± 0.6 fm for a_{nn} . Uncertainties in the neutron detector efficiencies and the integrated target-beam luminosity account for about 80% of the systematic uncertainty.

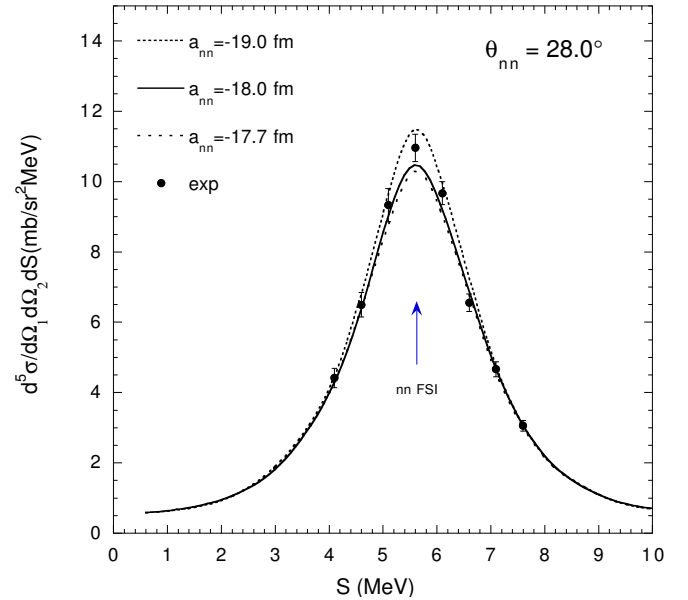


FIG. 3. Cross sections for $\theta_{nn} = 28.0^\circ$ ($\theta_{n1} = \theta_{n2} = 28.0^\circ$, $\phi_{12} = 0^\circ$). The points are the data from the present work. The curves are MC simulations based on nd calculations made with three values of a_{nn} : -17.7, -18.0, and -19.0 fm.

We observed no significant angle dependence in a_{np} , and the consistency in the a_{nn} data from one angle to the next is statistically acceptable. Combining the statistical and systematic uncertainties in quadrature, we obtain $a_{np} = -23.5 \pm 0.8$ fm and $a_{nn} = -18.7 \pm 0.6$ fm. Our result for a_{np} is in agreement with the value of a_{np} (-23.748 ± 0.009 fm [8]) obtained from free np scattering measurements. We use this result to set an upper limit on the influence of 3NF on the value of NN scattering lengths determined from our experiment, i.e., $\Delta a_{np}^{3NF} \leq a_{np}^{nd} - a_{np}^{free} = 0.2 \pm 0.8$ fm, where *free* and *nd* refer to values obtained from data for free np scattering and from nd breakup, respectively. This result is consistent with zero. Scaling our result for a_{np} by the ratio of a_{nn} to a_{np} , we obtain the upper limit due to 3NF effects in the nd breakup reaction to be $\Delta a_{nn}^{3NF} \leq 0.2 \pm 0.6$ fm, which is also consistent with zero.

Using the TM 3NF model we estimated possible effects of 3NF on np FSI cross sections. The calculations were produced by solving Eq.(2) using four modern NN potentials: AV18 [3], CD Bonn [14], NijmI and NijmII [15]. In each calculation the 2π -exchange TM 3NF potential [7] was included as V_4 , which was split into 3 parts where each one was symmetrical under exchange of two particles. For instance, for the 2π -exchange 3NF [7], this corresponds to the three possible choices of the nucleon which undergoes the (off-shell) $\pi - N$ scattering. In our calculations with the 3NF the strong cut-off parameter Λ in the TM 3NF model was adjusted separately for each NN potential to reproduce the experimental triton binding energy [16]. For details of the formalism and the numerical treatment refer to refs. [10,17]. We calculated the percentage deviation caused by effects of the TM 3NF on the np FSI point-geometry cross section as the function of θ_{np} at an incident neutron energy of 13 MeV. At all angles and for all potentials the change in the cross section due to the addition of the TM 3NF never exceeds 6%. For the np FSI production angles of the present experiment it is limited to the range of 1% to 4%, which corresponds to a theoretical range of $(\Delta a_{np}^{3NF})_{th}$ from -0.8 to -0.2 fm. Our experimentally determined Δa_{np}^{3NF} is within two standard deviations of the predictions using any of the four NN potentials with the TM 3NF adjusted to fit the triton binding energy.

TABLE I. The a_{np} and a_{nn} values extracted from the fit to the present data for the absolute NN FSI cross section in nd breakup at the angles measured in the present study. The χ^2 per datum for the best is given at each angle. The weighted mean of the data for all angles is given in the bottom row. All uncertainties are statistical only.

θ_{NN}	a_{np} (fm)	χ^2/pt	a_{nn} (fm)	χ^2/pt
43.0°	-23.6 ± 0.3	2.1	-18.8 ± 0.4	1.5
35.5°	-23.2 ± 0.3	2.7	-17.7 ± 0.4	0.6
28.0°	-23.7 ± 0.3	3.0	-18.8 ± 0.2	0.1
20.5°			-18.9 ± 0.2	0.8
Mean	-23.5 ± 0.2	2.6	-18.7 ± 0.1	0.6

Summarizing, our measured values are $a_{np} = -23.5 \pm 0.8$ fm and $a_{nn} = -18.7 \pm 0.6$ fm. In our analysis magnetic interactions are not considered. Their possible effects [18] have to be studied. By comparing our results for a_{np} to the recommended value from np free scattering and scaling by the ratio of a_{nn} to a_{np} , we set an upper limit of $\Delta a_{nn}^{3NF} = 0.2 \pm 0.6$ fm on the contribution of 3NF effects on our value of a_{nn} . Though the experimental results suggest an opposite sign for Δa_{np}^{3NF} than predicted using the TM 3NF, our value is consistent with the theoretical predictions within the reported uncertainties. Since our value for a_{np} obtained from nd breakup agrees with that from free np scattering, we conclude that

our investigation of the nn FSI done under identical conditions should lead to a valid measure of a_{nn} . Our value for a_{nn} is in agreement with the recommended value [2], which comes from π^-d capture measurements, and disagrees with values obtained from earlier nd breakup studies [1].

ACKNOWLEDGMENTS

This work was supported in part by the U.S. Department of Energy, Office of High Energy and Nuclear Physics, under grant No. DE-FG02-97ER41033, by the Maria Skłodowska-Curie II Fund under grant No. MEN/NSF-94-161, by the USA-Croatia NSF Grant JF129, and by the European Community Contract No. CII*-CT-91-0894. The numerical calculations were performed on the Cray T916 of the North Carolina Supercomputing Center at the Research Triangle Park, North Carolina and on the Cray T90 and T3E of the Höchstleistungsrechenzentrum in Jülich, Germany.

-
- [1] I. Šlaus, Y. Akaishi and H. Tanaka, Phys. Reports **173**, 259 (1989).
 - [2] G.A. Miller, B.M.K. Nefkens and I. Šlaus, Phys. Reports **190**, 1 (1990).
 - [3] R.B. Wiringa, V.G.J. Stoks and R. Schiavilla, Phys. Rev. C **51**, 38 (1995).
 - [4] B. Gabboud *et al.*, Phys. Rev. Lett. **42**, 1508 (1979).
 - [5] O. Schori *et al.*, Phys. Rev. C **35**, 2252 (1987).
 - [6] C.R. Howell *et al.*, Phys. Lett. B **444**, 252 (1998).
 - [7] S. A. Coon *et al.*, Nucl. Phys. A **317**, 242 (1979); S. A. Coon and W. Glöckle, Phys. Rev. C **23**, 1790 (1981).
 - [8] L. Koester and W. Nistler, Z. Physik, **272**, 189 (1975).
 - [9] H. Witała *et al.*, Phys. Rev. C **52**, 1254 (1995).
 - [10] W. Glöckle, H. Witała, D. Hüber and J. Golak, Phys. Reports **274**, 107 (1996).
 - [11] E. Finckh *et al.*, Nucl. Instr. and Meth. A **262**, 441 (1987).
 - [12] R. Machleidt, Adv. Nucl. Phys. **19**, 189 (1989); *ibid*, private communications.
 - [13] H. Witała, W. Glöckle and H. Kamada, Phys. Rev. C **43**, 1619 (1991).
 - [14] R. Machleidt, F. Sammarruca, and Y. Song, Phys. Rev. C **53**, R1483 (1996).
 - [15] V. G. J. Stoks, R. A. M. Klomp, C. P. F. Terheggen, and J. J. de Swart, Phys. Rev. C **49**, 2950 (1994).
 - [16] A. Nogga, D. Hüber, H. Kamada and W. Glöckle, Phys. Lett. B **409**, 19 (1997).
 - [17] D. Hüber, H. Kamada, H. Witała and W. Glöckle, Acta Phys. Polonica, B **28**, 1677 (1997).
 - [18] R.J. Slobodrian, Phys. Lett. B **135**, 17 (1984).